Disorder-induced bulk superconductivity in $ZrTe_3$ single crystals via growth control

Xiyu Zhu,[1,*] Bing Lv,[1,*] Fengyan Wei,[1] Yuyi Xue,[1] Bernd Lorenz,[1] Liangzi Deng,[1] Yanyi Sun,[1] and Ching-Wu Chu[1,2,†]

[1]*Texas Center for Superconductivity and Department of Physics, University of Houston, Houston, Texas 77204-5002, USA*

[2]*Lawrence Berkeley National Laboratory, Berkeley, California 94720, USA*

(Received 16 October 2012; revised manuscript received 28 December 2012; published 10 January 2013)

Layered $ZrTe_3$ crystallizes in an unusual structure that consists of both quasi-one-dimensional and quasi-two-dimensional features, conducive to the formation of charge-density wave and superconductivity, respectively. Bulk superconductivity up to 4 K in single crystalline samples of layered $ZrTe_3$ has been successfully induced through high growth temperature. This procedure induces atomic disorders at both the Zr and the Te1 sites, as evident from the x-ray-diffraction study. As a result, the charge-density wave is partially suppressed without chemical doping or pressurization. The observation helps to understand the peculiar superconductivity of $ZrTe_3$ and suggests a new path for the induction of superconductivity in complicated compounds with competitive orderings.

DOI: 10.1103/PhysRevB.87.024508 PACS number(s): 74.70.Dd, 71.45.Lr, 74.10.+v

I. INTRODUCTION

Coexistence of and competition between superconductivity (SC) and charge-density wave (CDW) has been one of the hot topics in solid-state chemistry and condensed-matter physics. Among all CDW-bearing materials,[1–3] the zirconium compound $ZrTe_3$, which was discovered in the 1970s and belongs to the family of quasi-two-dimensional MX_3 (transition-metal trichalcogenides), has attracted intensive attention due to its novel structural and unusual physical properties.[4,5] $ZrTe_3$ crystallizes in the TiS_3-type structure (space group $P2_1/m$), as shown in Fig. 1. The $ZrTe_3$ trigonal prisms as building blocks stack along the b direction and form an infinite quasi-one-dimensional chain. The Te(1) atoms are the prism caps, and form quasi-two-dimensional Zr-Te layers along the ac plane. On the other hand, almost linear Te-Te chains formed from the Te(2) and Te(3) atoms due to the stacking of the $ZrTe_3$ trigonal prism with alternating shorter (2.79 Å) and longer (3.10 Å) distances are found along the a-axis direction. Therefore, both the quasi-one-dimensional chains and the quasi-two-dimensional structural features coexist in the unit cell, and thus lead to a complicated Fermi surface with at least two principal sheets: a central three-dimensional (3D) hole-sheet corresponding mainly to the ($ZrTe_3$) columns, and the quasi-1D electron sheets associated with the Te(2)-Te(3) chains.[6] Band structure calculations[7,8] and angle resolved photoemission spectroscopy (ARPES) measurements[9,10] further indicate that these quasi-1D sheets are instable against some nesting of the $5p$ electron. A general valence description of $(Zr^{4+})(Te^{2-})(Te_2{}^{2-})$ and $(Zr^{2+})(Te^{2-})(Te_2)$ has been proposed as a simple explanation for the charge distortions along the $5p$ Te(2)-Te(3) chain direction.[7] Indeed, $ZrTe_3$ has a CDW transition at ∼70 K, which appears as a resistivity anomaly along the a axis, but not along the b directions.[11,12]

The superconductivity reported previously for $ZrTe_3$, is rather peculiar,[11–14] presumably due to the competitions from the CDW excitations. Although the resistance (R) drops along the a axis with an onset at 5–3.5 K is noticeable, typical bulk superconducting characteristics, such as the diamagnetic signal and clear specific heat anomaly, have been observed only below 1.5 K.[13,14] Neither R drop along the b axis nor a clear diamagnetic signal is detectable above 2 K. Therefore, the reported superconductivity above 1.5 K can be interpreted as filamentary at best, although its exact nature is still a puzzle. To further explore this issue, it will be very beneficial to convert the filamentary into ordinary bulk superconductivity by various methods. For example, bulk superconductivity has been found at 3.8 K with the intercalation of Cu or Ni.[15,16] However, such intercalation alters the chemical potential which affects both the Fermi-surface topology and the lattice distortions, and therefore would also change the CDW pinning and the carrier scattering in the system. To clarify the origin, methods other than ion intercalation are desired. As it is known that lattice defects can also pin and suppress CDW without the introduction of carriers,[17] we herein report the induction of bulk SC up to 4 K in the undoped $ZrTe_3$ single crystals through high-temperature synthesis, demonstrating that structural disorders induced through growth-temperature control can also suppress the CDW and induce bulk superconductivity up to ∼4 K in undoped $ZrTe_3$. Our data also demonstrate that the increase in density of states (DOS) through the suppression of CDW is the main factor behind the filamentary to bulk superconductivity evolution.

II. EXPERIMENT

Single crystals of $ZrTe_3$ are synthesized by reacting Zr and Te through the chemical vapor transport method with iodine as the transport agent. Different synthesis temperatures have been tried, e.g., at high temperature (HT)-950 °C (source)/850 °C (sink); and at low temperature (LT)-735 °C (source)/660 °C(sink). Chemicals are used as received: Zr (Alfa, powder), Te (Alfa, lump, 99.999%), and iodine (Alfa, pieces, 99.999%). The reaction of $ZrTe_3$ is exothermic, therefore it forms at the low-temperature end. All of the reaction tubes are restricted to 9 cm length. The total reagents of Zr and Te ∼0.2 g are pressed as a pellet and with 25 mg of iodine added. The HT-$ZrTe_3$ crystals are obtained using zirconium, tellurium, and iodine as the reaction source for two weeks at 950 °C(source)/850 °C (sink). The LT-$ZrTe_3$ crystals are synthesized at 735 °C (source)/660 °C (sink). All of the preparative manipulations are carried out in a purified argon atmosphere glove box, which maintains a total O_2 and H_2O level <1 ppm.

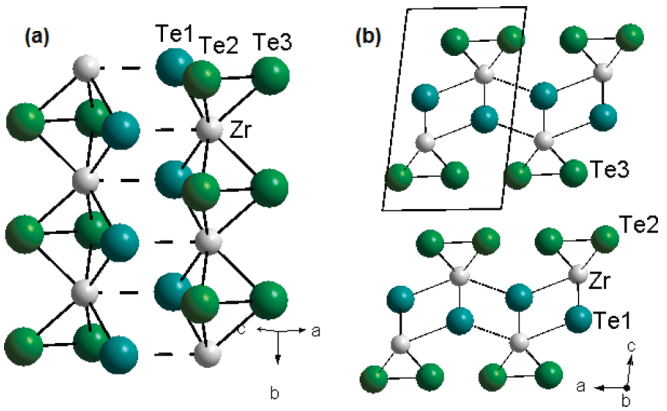

FIG. 1. (Color online) Crystal structure of $ZrTe_3$. (a) The quasi-one-dimensional $ZrTe_3$ trigonal prism packing along the b axis. (b) The quasi-two-dimensional $ZrTe_3$ layer along the a-c plane.

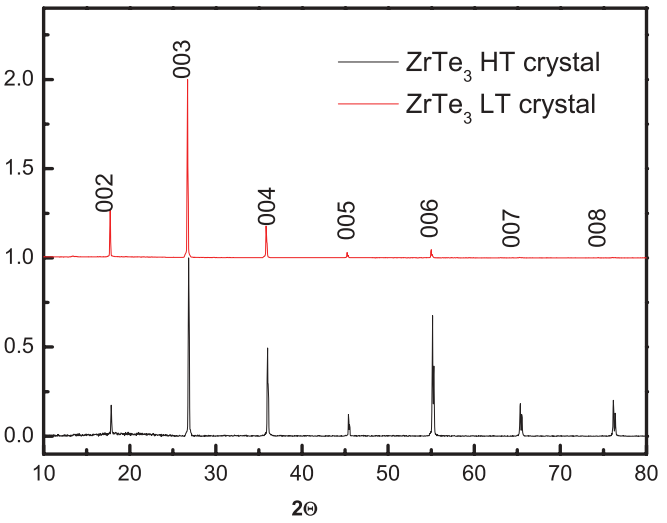

FIG. 2. (Color online) X-ray patterns of both HT- and LT-$ZrTe_3$ single crystals.

Crystalline samples are characterized by powder x-ray diffraction using a Rigaku DMAX III-B diffractometer. The chemical composition is determined by both energy dispersive x-ray spectroscopy (EDX) using a JEOL JSM-6330F field-emission scanning electron microscope and wavelength dispersive spectroscopy (WDS) on a JEOL JXA-8600 electron microprobe analyzer with 15 kV accelerating voltage, a 30-nA sample current, and 1-μm spot size. Precision of the results is smaller than 0.5% relative, and quoted errors reflect variations of count rates in multiple analyses of samples and exceed the precision of each individual analysis. The dc magnetic susceptibility is measured at ambient pressure using the Quantum Design magnetic property measurement system (MPMS) with a superconducting quantum interference device (SQUID) magnetometer in a field up to 5 T at a temperature down to 2 K. Electrical resistance as a function of temperature and field $R(T,H)$ is measured by employing a standard four-probe method using a Linear Research LR-400 ac bridge operated at 15.9 Hz in a Quantum Design physical property measurement system (PPMS) with fields up to 7 T.

Single-crystal x-ray diffraction of both HT and LT crystals is collected using a Siemens SMART APEX diffractometer equipped with a 1-K charge-coupled device (CCD) area detector. Graphite-monochromated Mo-K radiation (=0.710 73 Å) is used to collect a full hemisphere of data with the narrow-frame method. The data are integrated using the Siemens SAINT program, and the intensities corrected for Lorentz factor, polarization, air absorption, and absorption due to variation in the path length. Empirical absorption correction is applied using a shaped-lamina model, and redundant reflections are averaged. Final unit-cell parameters are refined using 626 reflections having $I > 10\sigma(I)$.

For the HT crystal, the cell parameters are $a = 5.917(5)$ Å, $b = 3.948(3)$ Å, $c = 10.155(8)$ Å, and $\alpha = 90°$, $\beta = 97.90(1)°$, $\gamma = 90°$. The structure is solved by direct methods with space group ($P2_1/m$) (no. 11) and refined by full-matrix least-squares calculations on $F2$; the thermal motion of all atoms are treated anisotropically. The final R indices are $[I > 2\sigma(I)]$, $R1 = 0.0510$, $wR2 = 0.1074$, $GOF = 0.948$, R indices (all data), $R1 = 0.794$, $wR2 = 0.1158$. All calculations are performed using the Siemens SHELXTL programs package.

III. RESULTS AND DISCUSSION

Long ribbonlike crystals with metallic luster and typical size of $5 \times 0.8 \times 0.2$ mm^3 are obtained. x-ray diffraction (XRD) results show the correct single crystalline TiS_3-type structure for both the HT- and LT-synthesized crystals with the c-axis preferred orientation as displayed in Fig. 2. Chemical analysis from energy dispersive x-ray spectroscopy (EDX) and wavelength dispersive spectroscopy (WDS) show the same stoichiometry ratio of Zr:Te $\sim$ 1:3 for both the HT and LT crystals; the difference of Zr/Te ratios lies in the uncertainty 0.5% of the WDS resolution, i.e., $Zr/Te = 1/3(1 \pm 0.5\%)$. There are no other impurity elements present from chemical analysis (as shown in Fig. 3).

The resistance (R) has been measured along the a and b axes (R_a and R_b) by the standard four-lead technique. We have chosen to present and discuss R, instead of resistivity, because of the large uncertainty in the effective dimensions of these needlelike crystals. The results of normalized $R_a(T)$ and $R_b(T)$ are displayed in Figs. 4(a)–4(c). For the LT crystal, it is evident from Fig. 4(a) that R_a decreases smoothly on cooling as a metal before a bump appears at a lower temperature, indicative of the onset of CDW at $T_{CDW} \approx 72$ K. The bump

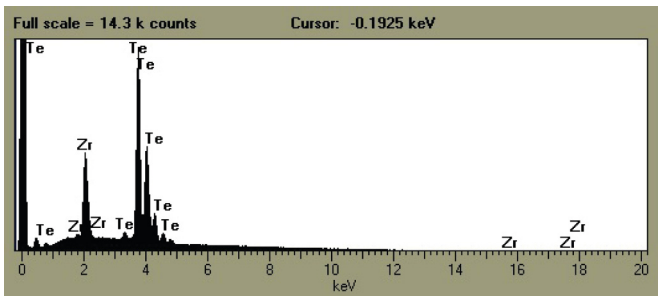

FIG. 3. (Color online) Energy dispersive x-ray spectroscopy of HT-$ZrTe_3$ single crystals.

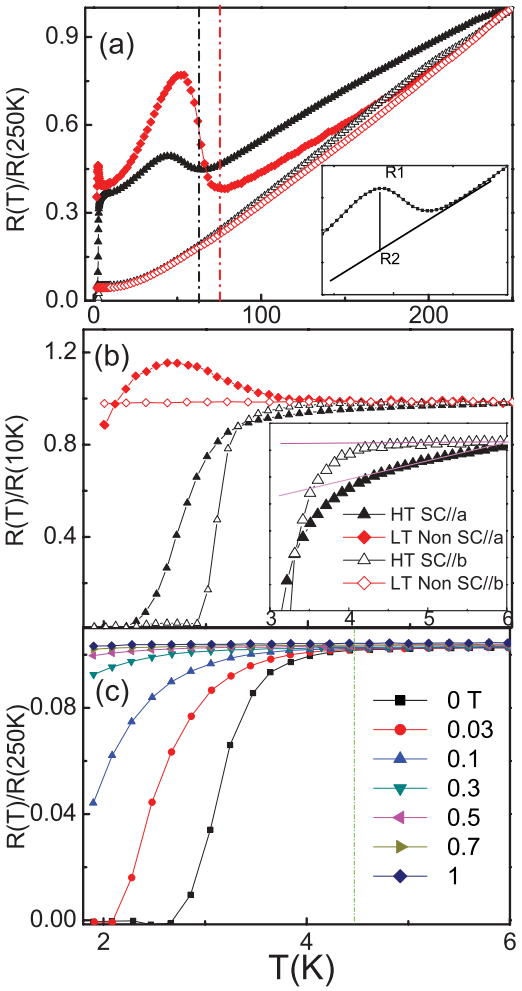

FIG. 4. (Color online) (a) Normalized temperature dependence of resistance of HT crystal (SC) and LT crystal (non-SC) along the a and b axes. Inset: the definition of $R1$ and $R2$, where $R1$ and $R2$ are the peak resistance of the bump and that expected in the absence of CDW, respectively. (b) Resistance normalized to 10 K. Inset: detail of resistance at the onset of SC HT crystal. (c) Normalized magnetoresistivity data along the b axis for HT crystal (SC) up to 1 T.

represents a depression of the DOS, which may be estimated as $\alpha = (R1 - R2)/R1 \approx 0.54$, where $R1$ and $R2$ are the peak resistance of the bump and that expected in the absence of CDW, respectively [as shown in inset of Fig. 4(a)]. With further cooling, $R_a(T)$ continues to decrease, rises at ~3.6 K, and decreases again only slightly but never reaches zero down to 2 K. $R_b(T)$, on the other hand, only decreases continuously and flattens out below 6 K. These results are consistent with and similar to earlier experiments, where the small R_a drop is taken as a sign for precursory filamentary SC.[13,14] The HT crystal behaves differently from the LT crystal but rather similar to the Ni- or Cu-doped $ZrTe_3$, as has been clearly observed. The CDW transition temperature is lowered to 61 K and the bump is significantly weakened with the estimated value $\alpha \approx 0.26$, comparable to that in $Cu_{0.05}ZrTe_3$ and $Ni_{0.05}ZrTe_3$.[15,16] More importantly, both $R_a(T)$ and $R_b(T)$ drop sharply to zero as the sample undergoes a superconducting transition with an onset T_{SC} up to ~4 K. In the presence of magnetic fields, the transition is broadened and suppressed to below 1.8 K at 1 T. This is in strong contrast to previous reports, in which only filamentary SC was detected along the a direction but not the b direction, indicating the different superconducting states in the HT and LT crystals.

To examine the nature of the SC transition, we have measured the dc magnetic susceptibility $\chi(T)$ of a HT crystal from 2 to 6 K. A clear diamagnetic transition to the superconducting state at 3 K is observed in both the zero-field-cooled χ_{ZFC} and the field-cooled χ_{FC} [see Fig. 5(a)]. The SC screen, therefore, has to be 3D up to 3 K. At 2 K and 4 Oe, the estimated shielding volume fraction, i.e., $4\pi\chi_{ZFC}$, is ~60% and the Meissner fraction $4\pi\chi_{FC}$ reaches ~18%, demonstrating that the superconducting state in the HT-$ZrTe_3$ crystal is indeed bulk. Both the nonperfect ~60% screen and

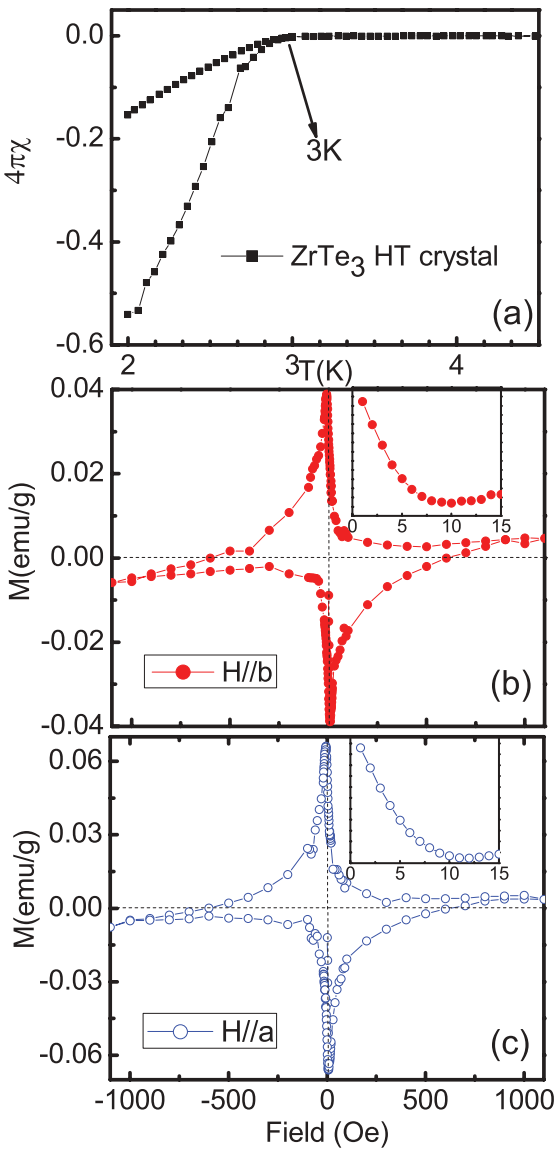

FIG. 5. (Color online) (a) ZFC and FC (4 Oe) magnetization susceptibility data of the superconducting $ZrTe_3$ HT crystal. (b) M-H curve at 2 K with $H \parallel b$. Inset: detail of the field scale between 0 and 15 Oe. (c) M-H curve at 2 K with $H \parallel a$. Inset: detail of the field scale between 0 and 15 Oe.

the broad transition demonstrate that the superconductivity of the crystals is highly inhomogeneous, which is rather natural considering the lattice disorders mentioned later. The magnetization (M) field (H) curves of another sample for H parallel to the a and b axes at 2 K in Figs. 5(b) and 5(c) demonstrate the type-II characteristic of the superconductor, with a lower critical field (H_{C1}) below 4 Oe. It is interesting to note that the maximum moment-split $\Delta M \approx 0.1$ emu/g observed is on the same order as the reported value of 0.06 emu/g in $Cu_{0.05}ZrTe_3$. Under Bean's model, this split is proportional to the critical current density and sample size.

Considering the high anisotropy of the compound, the apparent 3D screen discussed above can hardly be attributed to percolation paths. As an alternate check of the bulk superconducting property of the HT-$ZrTe_3$ crystal, we have measured the specific heat (C_P) under the earth field, and at 5 T. At 5 T, the superconductivity is completely suppressed,[15] as suggested by the linear C_P/T vs T^2 plot at 5 T [Fig. 6(a)]. Thus, the 5-T data are used as the normal-state reference line and the superconductivity is represented as $[C_P(0\ \mathrm{T}) - C_P(5\ \mathrm{T})]/T$ [Fig. 6(b)]. The data show a clear (though rather broad) superconductive peak up to 3 K. From the low-T approximation of $C/T = \gamma + \beta T^2$, both the residual carrier contribution γ_0 and the normal-state carrier contribution γ_n can be obtained from the intercepts of the associated C_P/T vs T^2 plots at 0 and 5 T, respectively. The data lead to $\gamma_0 = 1.1$ mJ/mol K^2, and $\gamma_n = 2.4$ mJ/mol K^2. Therefore, the superconducting volume fraction is estimated to be $(\gamma_n - \gamma_0)/\gamma_n = 54\%$, suggestive of a bulk SC instead of a filamentary SC or a minute impurity phase, consistent with the magnetic result. The broad transition and 54% volume fraction indicate that our samples are highly

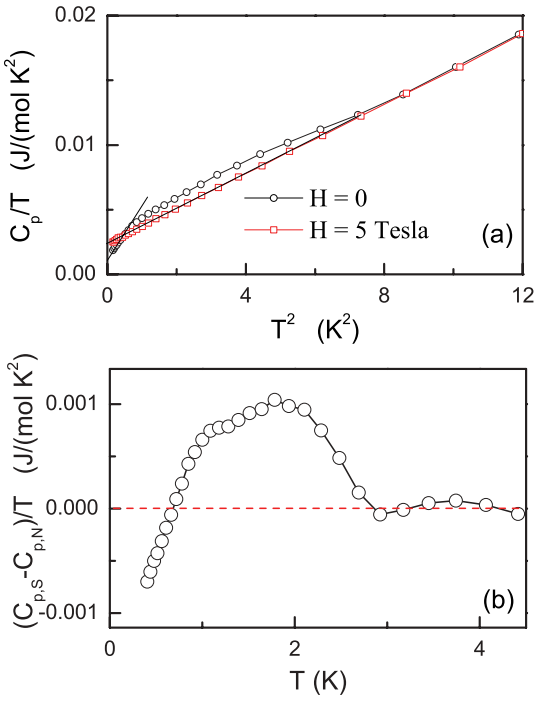

FIG. 6. (Color online) (a) (C_P/T) of HT $ZrTe_3$ crystal as a function of T^2 for $H = 0$, and $H \parallel c = 50$ KOe. (b) $(C_{P,S} - C_{P,N})/T$ as a function of T, where the data under 50 KOe are considered as the normal state.

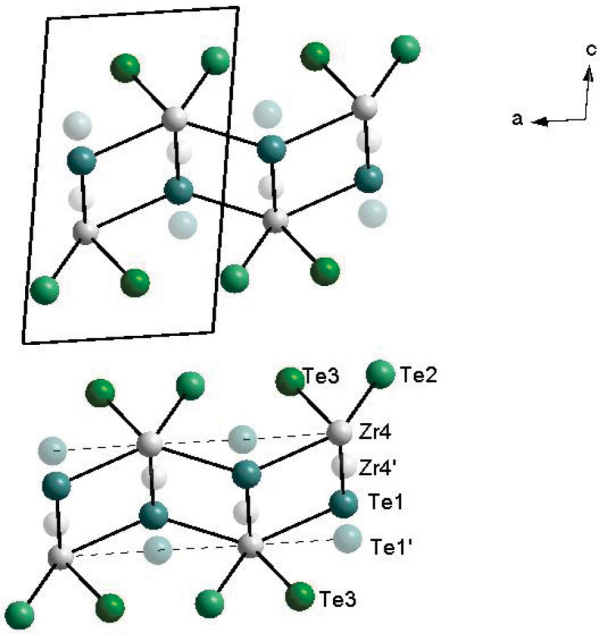

FIG. 7. (Color online) Single-crystal structure of HT $ZrTe_3$ sample, highlighting the disorder of the Zr and Te1 positions.

inhomogeneous due to the lattice disorder, which would be addressed below. The C_P anomaly observed is qualitatively similar to those observed in $Cu_{0.05}ZrTe_3$ and $Ni_{0.05}ZrTe_3$ with a broader distribution and smaller amplitude.[15,16] The Sommerfeld coefficient (γ_n) and the Debye temperature (θ_D) have been obtained from the C_P with values of 2.4 mJ/mol K^2 and 184 K, respectively.

As described above, both the HT- and LT-$ZrTe_3$ single crystals possess the same stoichiometry of Zr/Te = 1/3 and the same crystal structure of TiS_3 type, so the appearance of bulk superconductivity only in HT-$ZrTe_3$ crystals without chemical doping is indeed puzzling. Since the only difference between the two types of crystals lies in their synthesis temperatures, we conjecture that microstructure differences caused by the varied synthesis temperatures may be responsible for the divergence in superconductivity states.

To explore the cause of the bulk superconductivity observed, detailed crystal-structure investigation is carried out for both the HT- and LT-$ZrTe_3$ crystals. Both samples are found to crystallize with a monoclinic symmetry of ($P2_1/m$,♯11) as expected. The lattice parameters of the LT-$ZrTe_3$ crystal are found to be $a = 5.898(2)$ Å, $b = 3.924(1)$ Å, $c = 10.109(2)$ Å, and $\alpha = 90°$, $\beta = 97.88(3)°$, $\gamma = 90°$, consistent with the

TABLE I. Atom positions of the HT $ZrTe_3$ sample. Both Zr and Te1 positions split into two positions.

Atom	site	x	y	z	Occ.
Zr	2e	0.7122(4)	0.25	0.3343	0.907
Zr′	2e	0.749	0.25	0.4370	0.093
Te1	2e	0.2361(2)	0.25	0.4453	0.939
Te1′	2e	0.2010	0.25	0.337	0.061
Te2	2e	0.9053(3)	−0.25	0.1613(2)	1
Te3	2e	0.4314	−0.25	0.1670	1

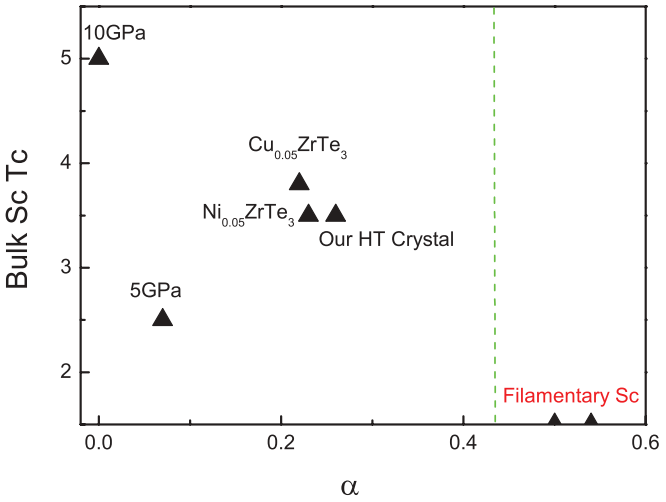

FIG. 8. (Color online) The relationship between bulk superconductivity and α. The high-pressure and intercalation data are from Refs. 15,16 and 19.

previous report.[7] On the other hand, the lattice parameters of HT-$ZrTe_3$ are found to be $a = 5.917(5)$ Å, $b = 3.948(3)$ Å, $c = 10.155(8)$ Å, and $\alpha = 90°$, $\beta = 97.90(1)°$, $\gamma = 90°$,[18] which is slightly larger than the unit cell of LT-$ZrTe_3$. Although the HT and LT crystals are rather similar structurally, significant variation in structural disorders at the Zr and the Te(1) positions is detected in the HT-$ZrTe_3$ crystals along the a-c plane (Fig. 7). As also shown in Table I, the Zr location splits into two positions with 91% and 9% occupancies, respectively. The two split sites are ~1.03 Å apart toward the Te(1) atom direction. Similarly, the Te(1) site also splits into two along the Te(1)-Zr direction; the splitting is ~1.09 Å with about 94% and 6% occupancies, respectively. Consequently, some of the Zr atoms move toward Te(1), and both the Zr-Te(2) and the Zr-Te(3) bonds are stretched. The distances of Zr′-Te(2) and Zr′-Te(3) become ~3.65(3) Å and 3.68(2) Å, respectively, compared to the Zr-Te(2) distance of 2.973(3) Å and Zr-Te(3) distance of 2.961(3) Å. The presence of such disorders in the HT crystals is consistent with the higher R (250 K) (not shown) and the smaller $R(250\ K)/R(72\ K)$ ratio of the HT crystal shown in Fig. 4(a). As a result, the charge distribution along the Te(2)-Te(3) chain locations could be altered, leading to the suppression of the CDW ordering. Therefore, bulk SC can be established up to 3–4 K through three different procedures, i.e., chemical intercalation such as with Cu or Ni, high pressure, and lattice disorders, if the CDW strength α is suppressed down below 0.3 (Fig. 8).[15,16,19] The data suggest that the peculiar superconductivity of $ZrTe_3$ is largely due to the depletion of DOS through competition with CDW. In addition, our data demonstrate that the lattice defect may promote superconductivity.

It is interesting to note that according to the reported phase diagram,[20] the $ZrTe_3$ should decompose to $ZrTe_2$ and Te above 630 °C. The crystal formation temperature (850 °C) of our work is much higher. Therefore, to confirm the importance of the synthesis temperature for the emergence of the bulk superconductivity, a small nonsuperconducting $ZrTe_3$ crystal is heated up to 850 °C in a sealed quartz tube for 10 h. No indication of decomposition or melting is observed. More significantly, a clear bulk superconductivity signal emerges from magnetic susceptibility measurements similar to HT $ZrTe_3$, further proving that the synthesis temperature is important for the appearance of the bulk superconductivity signal. Recently, Yadav *et al.* also reported the formation of the polycrystalline $ZrTe_3$ sample at 975 °C[21] which supports our results.

IV. CONCLUSIONS

Single crystals of $ZrTe_3$ have been synthesized at different temperatures with drastically different superconducting properties: bulk superconductivity in HT-$ZrTe_3$ crystals without doping up to 4 K, but not in LT-$ZrTe_3$ crystals, as evident from the resistive, magnetic, and calorimetric results. The difference can be attributed to the suppression of the CDW order through the growth-induced structural disorders at high temperature, which are clearly shown by our systematic x-ray-diffraction study. Our observations demonstrate that synthetic temperature could be used as a tuning parameter besides chemical doping and physical pressure to induce superconductivity and to vary charge-density waves in transition metal chalcogenides in general and in $ZrTe_3$ in particular.

ACKNOWLEDGMENTS

The work in Houston was supported in part by US Air Force Office of Scientific Research Contract No. FA9550-09-1-0656, US Air Force Research Laboratory Subcontract No. R15901 (CONTACT) through Rice University, the T. L. L. Temple Foundation, the John J. and Rebecca Moores Endowment, and the State of Texas through the Texas Center for Superconductivity at the University of Houston. The work at Lawrence Berkeley National Laboratory was supported by the Director, Office of Science, Office of Basic Energy Sciences, Division of Materials Sciences and Engineering of the US Department of Energy. Chemical analysis from J. Meen and helpful discussion with X. Wang are greatly appreciated.

*The first two authors contributed equally.
†cwchu@uh.edu

[1] J. A. Wilson and A. D. Yoffe, Adv. Phys. **18**, 193 (1960).
[2] A. H. Castro Neto, Phys. Rev. Lett. **86**, 4382 (2001).
[3] E. Morosan, H. W. Zandbergen, B. S. Dennis, J. W. G. Bos, Y. Onose, T. Klimczuk, A. P. Ramirez, N. P. Ong, and R. J. Cava, Nat. Phys. **2**, 544 (2006).
[4] L. Brattas and A. Kjekshus, Acta Chem. Scand. **26**, 3441 (1972).
[5] S. Furuseth, L. Brattas, and A. Kjekshus, Acta Chem. Scand. Ser. A **29**, 623 (1975).
[6] M. Hoesch, X. Cui, K. Shimada, C. Battaglia, Shin-ichi Fujimori, and H. Berger, Phys. Rev. B **80**, 075423 (2009).
[7] K. Stowe and F. R. Wagner, J. Solid State Chem. **138**, 160 (1998).

[8]C. Felser, E. W. Finckh, H. Kleinke, F. Rocker, and W. Tremel, J. Mater. Chem. **8**, 1787 (1998).
[9]T. Yokoya, T. Kiss, A. Chainani, S. Shin, and K. Yamaya, Phys. Rev. B **71**, 140504(R) (2005).
[10]P. Starowicz, C. Battaglia, F. Clerc, L. Despont, A. Prodan, H. J. P. van Midden, U. Szerer, A. Szytuta, M. G. Garnier, and P. I. Aebi, J. Alloys Compd. **442**, 268 (2007).
[11]S. Takahashi, T. Sambongi, and S. Okada, J. Phys. (Paris) Colloq. C **3**, 1733 (1983).
[12]D. J. Eaglesham, J. W. Steeds, and J. A. Wilson, J. Phys. C **17**, L697 (1984).
[13]H. Nakajima, K. Nomura, and T. Sambongi, Physica B **143**, 240 (1986).
[14]K. Yamaya, S. Takayanagi, and S. Tanda, Phys. Rev. B **85**, 184513 (2012).
[15]X. D. Zhu, H. C. Lei, and C. Petrovic, Phys. Rev. Lett. **106**, 246404 (2011).
[16]H. C. Lei, X. D. Zhu, and C. Petrovic, Europhys. Lett. **95**, 17011 (2011).
[17]H. Dai and C. M. Lieber, J. Phys. Chem. **97**, 2362 (1993)
[18]Crystallography data for the HT $ZrTe_3$ crystal: $a = 5.917(5)$ Å, $b = 3.948(3)$ Å, $c = 10.155(8)$ Å, and $\alpha = 90^\circ$, $\beta = 97.90(1)^\circ$, $\beta = 97.90(1)^\circ$, $Z = 2$; $V = 234.9(3)$ Å^3; $\mu = 20.390$ mm^{-1}; $\lambda = 0.710\,73$ Å; $2\theta_{\max} = 57.64$; total reflns = 1399; independent reflns = 626; observed $[I > 2\sigma(I)] = 626$; total variables = 35; $[I > 2\sigma(I)]$: $R1 = 0.0510$, $wR2 = 0.1074$, $GOF = 0.948$; all data: $R1 = 0.794$, $wR2 = 0.1158$. Data collected by a Siemens SMART diffractometer ($T = 25\,^\circ$C). Structure is solved by direct methods and refined by full-matrix least-squares calculations. All calculations are performed using SHELXTL.
[19]R. Yomo, K. Yamaya, M. Abliz, M. Hedo, and Y. Uwatoko, Phys. Rev. B **71**, 132508 (2005).
[20]R. de Boer and E. H. P. Cordfunke, J. Nucl. Mater. **223**, 103 (1995).
[21]C. S. Yadav and P. L. Paulose, J. Phys.: Condens. Matter **24**, 235702 (2012).